

## Dimensional Description of Cyclic Macromolecules

Gregory Beaucage\* and Amit S. Kulkarni

*Department of Chemical and Materials Engineering, University of Cincinnati, Cincinnati, Ohio 45221-0012*

*Received June 15, 2009; Revised Manuscript Received November 23, 2009*

**ABSTRACT:** Cyclic structures are often used to model and simulate long chain molecules due to the simplification of no chain-end effects. Many technically important and biologically relevant molecules are cyclics. Further, ring polymers display dramatic viscosity enhancement when blended with linear polymers in the melt. It has been proposed that cyclic melts may display a topologically driven coil collapse at high molecular weights reminiscent of cyclic DNA. Despite the structural simplicity and importance of cyclics a quantitative analytic distinction between cyclics and linear chains in the melt or in solution has been elusive since both linear and cyclic macromolecules display similar disordered, fractal structures. A dimensional analysis of cyclic polymers and its use to describe scattering data from cyclic macromolecules is presented. The validity of the new approach to describe cyclic structures is demonstrated using experimental data, and the Casassa form factor, previously used for cyclic polymers, is critically revisited. The scaling model is also used to quantify cyclic coil collapse in simulations from the literature.

### Introduction

Cyclic structures are prevalent in many biological and synthetic molecules; e.g. cyclic molecules play an important role in the DNA transcription process<sup>1</sup> as well as complex biochemical processes like insulin secretion.<sup>2</sup> Synthetic systems like macrocyclic-ethers (crown-ethers) have been synthesized for specific applications like cationic and anionic complexation agents.<sup>3,4</sup> Such macrocyclic crown-ethers have been used to thread polymers in an attempt to mimic biomolecular processes.<sup>5</sup> Cyclics also present model structures for the study of polymers since they lack the complication of chain-end effects.<sup>6</sup> However, the absence of chain ends has led to speculation that the dynamic properties of polymeric rings differ from their linear analogues.<sup>7–9</sup> Recent studies have shown dramatic enhancement of viscosity when a small amount of linear chains are added to cyclic polymers.<sup>10,11</sup>

The structural characterization of cyclic macromolecules includes detailed experimental studies conducted on cyclic poly-(dimethylsiloxane) (PDMS).<sup>12–14</sup> PDMS displays a natural tendency to form rings during synthesis. Small angle neutron scattering (SANS) has been a primary tool to quantify these structures, and has made it possible to corroborate theoretical/computational predictions regarding the structure/conformation of ring polymers under different thermodynamic conditions.<sup>7–10,15–18</sup> These studies along with the recent development of Ru-based catalyst systems by Bielawski et al.<sup>19</sup> for industrial scale production of cyclic polymers has invigorated interest in obtaining effective descriptions of cyclic structures.

SANS is a useful analytic technique to characterize features of the structure like the mean square radius of gyration of the cyclic macromolecule,  $R_g$ , as well as the mass/size scaling of such a structure. The Casassa form factor<sup>20</sup> has been used for cyclic macromolecules. It has been reported<sup>12</sup> that the Casassa equation results in less than satisfactory fits to describe the observed small angle scattering (SAS) patterns, especially for cyclics of high molar mass.

\*Corresponding author.

This paper describes a pathway to model cyclics using a new approach developed by Beaucage<sup>21–26</sup> for analyzing hierarchical structures. Literature SANS data from cyclic polymers and simulated structure factors from the literature will be used as a check for this approach. It will be evident that this model yields an effective description for cyclic polymers. New information regarding the conformational and thermodynamic states of cyclics can be understood using this approach. A latter section will critically assess the Casassa equation<sup>20,27,28</sup> using this new structural model.

### Scaling Model for Cyclic Structures

A cyclic macromolecule displays tortuosity of the chain path associated with thermodynamic conditions and structural constraints on chain randomness. The cyclic also displays a fixed connectivity associated with the ring structure that is not changed by solvation conditions. These two features of cyclics can be described using a universal scaling model.<sup>21–26</sup> The scaling model describes a complex macromolecule composed of  $z$  primary units, of which  $p$  units describe the average *minimum* or *short circuit* path through the structure (broken line and lighter circles in Figure 1). The average minimum path is the average path of conduction or the path on which mechanical stress is transferred through the structure.  $p$  is related to the chain size  $R/l_K$  through the minimum dimension,  $d_{\min}$ , where  $R$  is the end-to-end length of the structure and of an average minimum path, and  $l_K$  is the Kuhn length or step size,

$$p = \left(\frac{R}{l_K}\right)^{d_{\min}} \quad (1)$$

Equation 1 describes the tortuosity of the structure. A structure with no tortuosity displays  $d_{\min} = 1$  and a minimum in  $p$  for a given  $R/l_K$ . Both  $p$  and  $d_{\min}$  increase with increasing tortuosity of the chain path. The connectivity of a complex structure can be described by the connecting path,  $s$ , that links chain ends and

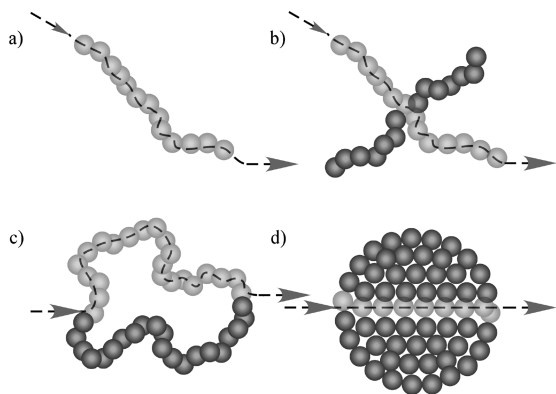


**Figure 1.** Schematic representation of the minimum path,  $p$ , through a cyclic structure (1c) as discussed in text. The minimum path for a cyclic would constitute half the chain (indicated by the broken line and lighter circles): (a) linear chain, (b) 4-arm star, (c) cyclic, and (d) disk.

branch/junction sites with straight lines. In analogy to eq 1 we can write

$$s = \left(\frac{R}{l_K}\right)^c \quad (2)$$

where  $c$  is the connectivity dimension. For a linear chain  $c = 1$  and  $s$  is a minimum for a given  $R/l_K$ . For the chain mass,  $z$ , we can also write

$$z = \left(\frac{R}{l_K}\right)^{d_f} = p^c = s^{d_{\min}} \quad (3)$$

where  $d_f$  is the mass fractal dimension and

$$d_f = c d_{\min} \quad (4)$$

$(z - p)$  units are present in structural branches, so the branch fraction  $\phi_{Br}$  is given as<sup>21</sup>

$$\phi_{Br} = \frac{z - p}{z} = 1 - z^{1/c - 1} \quad (5)$$

By analogy we can also define a “meandering” fraction that accounts for mass that is not used in direct, linear connectivity,

$$\phi_M = \frac{z - s}{z} = 1 - z^{1/d_{\min} - 1} \quad (6)$$

$\phi_{Br}$  can be quantitatively obtained for a variety of different molecular architectures using SAS.<sup>21–26</sup>

The scaling model can be adapted to describe a cyclic structure. As seen in Figure 1, the minimum path for an uncollapsed cyclic structure is composed of half its length ( $p = z/2$ ); so, from eq 3

$$\frac{1}{c} = 1 - \frac{\ln 2}{\ln z} \quad (7)$$

$c$  is a function of  $z$  and approaches 1 (the definition of a linear chain) for large  $z$ . Further, eq 7 indicates that the cyclic has the topology of a disk ( $c = 2$ ) when the cyclic is composed of 4 units ( $z = 4$ ). An expression for  $d_{\min}$  can be obtained by combining eqs 4 and 7

$$d_{\min} = d_f \left(1 - \frac{\ln 2}{\ln z}\right) \quad (8)$$

The mass-fractal dimension for cyclics,  $d_f$ , cannot be calculated by this method since the chain’s mass-fractal scaling is perturbed from the thermodynamically limiting values of 2 for  $\Theta$  conditions and  $\sim 3/3$  for good solvents by the cyclic connectivity. That is, we cannot assume that a comparable linear chain of  $z/2$  units has these thermodynamically limiting values of the mass-fractal dimension for a cyclic structure.

Cates and Deutsch<sup>7</sup> indicate that a cyclic in the melt is restricted from certain topologically excluded conformations associated with concatenation and knotting. This leads to a reduction in size compared to a linear chain and an increase in the free energy. The topologically driven size reduction is opposed by the chain’s entropic elasticity. A simple free energy expression based on these two terms can be minimized to yield a mass-fractal dimension of 2.5 for a cyclic in the melt. Modification of these topological restrictions could reduce the  $d_f$  to about 2.2 which is observed in simulations<sup>15–18</sup> and close to what was observed experimentally for cyclic PDMS melts.<sup>12–14</sup>

The primary particles that do not compose the average minimum path contribute toward  $\phi_{Br}$ . Hence, for cyclic structures  $\phi_{Br}$  should display a constant value of 0.5 (Figure 1), regardless of molar mass,  $z$ .

In the context of this scaling model it is interesting to compare a symmetric 4-arm star and a cyclic polymer, since both these structures display  $\phi_{Br} = 0.5$ . This is indicated schematically in Figure 1b and 1c.  $d_{\min}$  and  $c$  follow the same functions for the 4-arm star and cyclic. The structures are distinguished by their  $R_g$ ’s,  $R_{g,cyclic}^2 = R_{g,linear}^2/2$  and  $R_{g,4-star}^2 = R_{g,linear}^2/1.6$  from eqs 6.28 and 6.85 of ref 28 for Gaussian scaling.

For a cyclic melt there are two main topological features, the ring structure itself, that is, any step of the chain is indistinguishable from any other step; and the absence of concatenation or linking of the rings mentioned above. These two features are distinguished in the scaling model by the constraints of eqs 7 and 8 and by the value of  $R_g$  given below by eq 13 for nonconcatenated cyclics. Equations 8 and 13 also involve the chain tortuosity and flexibility through the value of  $d_{\min}$ . The chain tortuosity is partly controlled by steric constraints, and thermodynamic conditions. The final coil size is influenced both by topology as well as tortuosity.

Simulations of cyclic melts have shown that a scaling transition may occur in molecular weight leading to coil collapse at high molecular weight that is driven by the topological constraints mentioned above.<sup>15–18</sup> The transition from an expanded coil to a globular structure is easily distinguished in the context of the scaling model by a decrease in  $d_{\min}$  to 1 for a globular structure and an increase in  $c$  toward 3, as well as an increase in  $\phi_{Br}$  to 1 for a 3d object. It is expected that as the cyclic approaches a globular state the connectivity will increase similar to what has been observed for proteins and RNA during folding as demonstrated in a previous publication.<sup>24</sup>

The scaling model can accommodate a variety of structural changes including changes in connectivity associated with coil collapse as described in ref 24. Equations 7 and 8 rely on a noncollapsed coil, so it is expected that deviations from these functions will be observed during cyclic globule formation, particularly, a relative increase in  $c$  and decrease in  $d_{\min}$ . Observation of these deviations at high molecular weight would be consistent with topology driven cyclic collapse at high molecular weight predicted in the literature.<sup>15–18</sup> It is also expected that  $\phi_{Br}$  would increase from 0.5 as coil collapse progresses.

### Small-Angle Scattering

The scattering curve from a mass-fractal object, of which a cyclic is an example, displays two regimes. At low- $q$ , the Guinier regime follows<sup>29–31</sup>

$$I(q) = G \exp\left(-\frac{q^2 R_g^2}{3}\right), \quad (9)$$

and at high- $q$  the mass-fractal power law regime follows,

$$I(q) = B_f q^{-d_f} \quad (10)$$

where  $I$  is the scattered intensity,  $q$  is the scattering vector given as  $q = 4\pi \sin(\theta/2)/\lambda$ ,  $\theta$  is the scattering angle,  $\lambda$  is the wavelength of

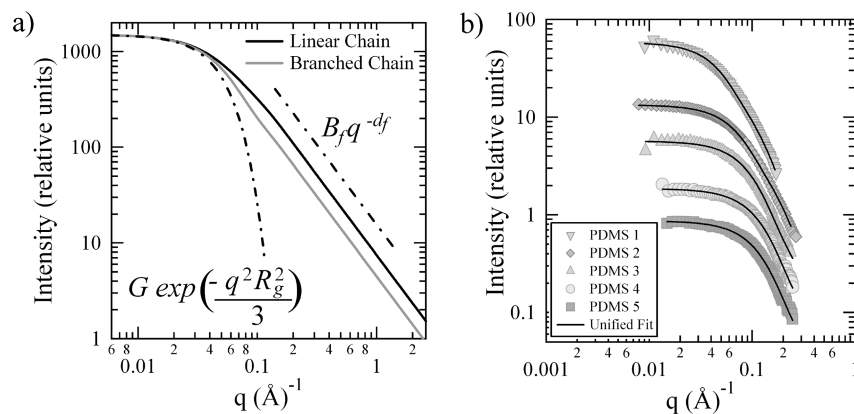


**Figure 2.** (a) Unified small-angle scattering calculation<sup>21,29–31</sup> for hierarchical linear (black curve) and branched (gray curve) structures. (b) Digitized small angle neutron scattering data from blends of hydrogenous and deuterated cyclic PDMS samples from literature.<sup>12–14</sup> The details of the samples are given in Table 1. The data are fit to the unified function.<sup>21,29,30</sup>

**Table 1. Description and Fit Results for Poly(dimethylsiloxane) (PDMS) Samples<sup>a</sup>**

sample	$M_w$ (g/mol) <sup>12–14</sup>	$G$	$R_g$ (Å)	$B_f$	$d_f$	$\phi_H$
PDMS 5 [Figure 6a in ref 12]	4780/4760	3.9	13.6	0.0214	2.11	0.26
PDMS 4 [Figure 1b in ref 14]	5000/5000	3.9	13.6	0.0210	2.12	0.50
PDMS 3 [Figure 6b in ref 12]	4780/11 140	5.6	16.8	0.0185	2.16	0.26
PDMS 2 [Figure 14 in ref 13]	8900/11 110	6.2	20.3	0.0183	2.07	0.66
PDMS 1 [Figure 13 in ref 13]	19 800/16 300	12.6	30.6	0.0155	2.11	0.52
Casassa					~2.12	

<sup>a</sup> Casassa refers to values from a fit of eq 14.

the radiation,  $G$  and  $B_f$  are the Guinier and power law prefactors, respectively, and  $R_g$  is the radius of gyration of the polymer coil. Figure 2a shows the origin of the four free parameters obtained from SANS:  $G$ ,  $R_g$ ,  $B_f$ , and  $d_f$ .  $G$  and  $R_g$  are derived from Guinier's law (eq 9), which predicts an exponential decay in scattered intensity associated with the overall  $R_g$  of the structure (dot-dash curve to the left of Figure 2a), and  $B_f$  and  $d_f$  reflect the power law (dot-dash curve to the right of Figure 2a) which gives the mass/size scaling of the structure in terms of the mass-fractal dimension  $d_f$  (eq 10). Beaucage<sup>21</sup> has shown that the topology of the structure, as described by the scaling model, can be quantitatively measured by combining parameters from these two scattering regimes.  $d_{\min}$ , for example, can be calculated as<sup>21</sup>

$$d_{\min} = \frac{B_f R_g^{d_f}}{G(\Gamma^{d_f/2})} \quad (11)$$

where  $\Gamma$  is the gamma function. With  $d_f$  from eq 10 and using eq 4,  $c$  can be obtained.  $p$  and  $s$  can be obtained from  $z$  using eq 3.

Rather than free fits to determine the scaling features, a scattering function for cyclics can also be proposed from this scaling method using the unified function<sup>21,29,30</sup> and  $B_f$  obtained from eqs 8 and 11

$$B_{f, \text{cyclic}} = \frac{d_{\min} G(\Gamma^{d_f/2})}{R_g^{d_f}} = \frac{d_f G \left(1 - \frac{\ln 2}{\ln z}\right) (\Gamma^{d_f/2})}{R_g^{d_f}} \quad (12)$$

$z$ , the number of Kuhn steps, can be obtained by several methods such as from  $R_g$  (used here), from a comparison of the persistence and coil scattering<sup>25,26</sup> and from an independent measurement of the molecular weight. In this paper  $c$  will be measured, using eqs 11 and 4 to determine agreement with the expected value of eq 7.

Figure 2a also shows the signature effect of the topological structure on SANS data. The black curve represents SANS from a linear structure for which  $z = p$ ,  $d_{\min} = d_f$  and  $c = 1$ . The gray curve represents scattering from a "regular" structure for which  $z \gg p$ ,  $d_{\min} = 1$ , and  $c = d_f$ . Topology is thus reflected by a shift of the power law relative to Guinier's law, and is quantifiable (eqs 11 and 12).

### Cyclic PDMS

SANS data from blends of hydrogenous ( $H$ ) and deuterated ( $D$ ) cyclic PDMS, digitized from the literature are shown in Figure 2b.<sup>12–14</sup> The details of the PDMS samples are given in Table 1. The first column in Table 1 indicates the sample name and the reference and figure from which the data was obtained.  $\phi_H$  in Table 1 indicates the mole fraction of the hydrogenous component. The SANS data are fit to the unified function<sup>29,30</sup> that incorporates eqs 9 and 10 assuming that blends of  $H$  and  $D$  PDMS constitute an athermal mixture,<sup>32</sup>  $\chi = 0$ , and assuming that the individual structure factors (for  $H$  and  $D$  components) have the same  $R_g$ .<sup>34</sup> The results of these fits are tabulated in Tables 1 and 2.

Calculation of  $\phi_{B_f}$  requires the number of Kuhn steps,  $z$ .  $z$  is obtained from  $R_g$ ,  $d_{\min}$  and the Kuhn length,  $l_k = 2 l_p/z$ , where  $l_p$  is the persistence length. For PDMS,  $l_p = 5.61$  Å.<sup>33,36–39</sup>  $z$  is calculated from eq 6 of ref 30

$$z = 2 \left( \frac{R_g^2 \left(1 + \frac{2}{d_{\min}}\right) \left(2 + \frac{2}{d_{\min}}\right)}{4kl_p^2} \right)^{d_{\min}/2}, \quad (13)$$

assuming that  $z$  for the cyclic is twice  $z$  for a linear chain having the same  $R_g$  and mass fractal dimension  $d_{\min}$ , due to symmetry of the structure on average about any two points separated by  $z/2$

units.  $k$  in eq 13 is a constant that is on the order of 1. Equation 13 reduces to  $R_{g,cyclic}^2 = R_{g,linear}^2/2$  when  $d_{min} = 2$  in agreement with eq 6.28 of ref 28.

The  $\phi_{Br}$  values for all the cyclic samples calculated from eq 6 are close to 0.5 (Table 2). The calculations are performed for  $k = 1.89$  in eq 13 which is a value that results from comparison of the observed  $c$  values and those predicted by eq 7 as discussed below.  $k$  depends on the chemical structure.  $k$  was found to have a value of 1.75 for polyethylene<sup>25</sup> and  $k$  was found to be 2.6 for polyurethane.<sup>40</sup>

$d_{min}$ , in Table 2, increases with increasing molecular weight of the cyclic PDMS blends from 1.37 to 1.72, asymptotically approaching the mass/size scaling of a linear chain in the melt (Gaussian,  $d_{min} = d_f = 2$ ).<sup>6</sup> The observed values of  $d_{min}$  are lower

**Table 2. Calculated Values for PDMS Samples:  $d_{min}$ ,  $c$ ,  $z$ , and  $\phi_{Br}$ <sup>a</sup>**

sample	$d_{min}$	$c$	$z$	$k = 1.89 \phi_{Br}$	$\phi_M$
PDMS 5 <sup>12</sup>	1.37	1.54	7.31	0.50	0.42
PDMS 4 <sup>14</sup>	1.39	1.52	7.36	0.49	0.43
PDMS 3 <sup>12</sup>	1.51	1.43	10.5	0.51	0.55
PDMS 2 <sup>13</sup>	1.54	1.35	14.3	0.50	0.61
PDMS 1 <sup>13</sup>	1.72	1.23	32.9	0.48	0.77
Casassa	~1.36	~1.56	~6.9	~0.50	~0.40

<sup>a</sup> $k$  is from eq 13. Casassa refers to values from a fit of eq 14.

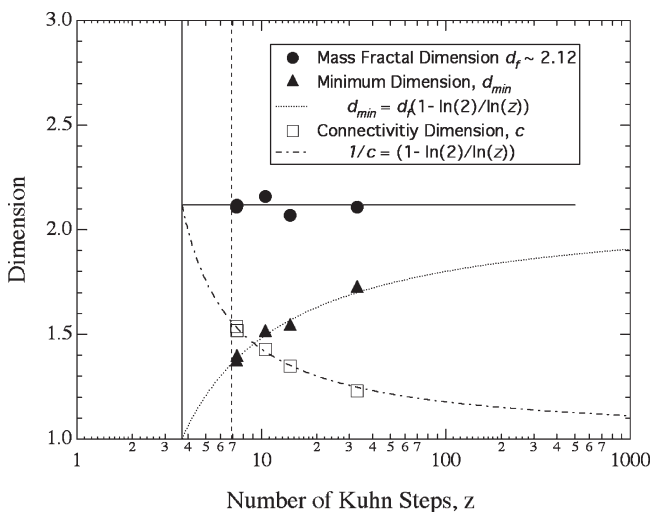


**Figure 3.** Mass fractal dimension, minimum dimension and connectivity dimension,  $c$ , from Table 2 using  $k = 1.89$  plotted as a function of the number of Kuhn units,  $z$ . The line through  $d_f$  is at a value of 2.12. The curves through  $c$  and  $d_{min}$  follow eqs 7 and 8. The vertical dashed line indicates the approximate values for eq 14 if  $p = z/2$ .

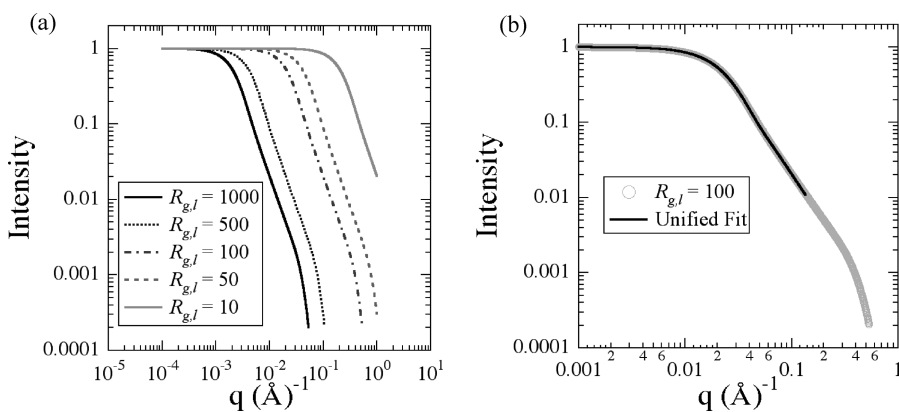


**Figure 4.** (a) Equation 14 for several values of the linear  $R_{g,l}$ . By scaling the  $q$  vector by  $R_{g,l}/100$  all of the curves collapse on the  $R_{g,l} = 100$  curve. (b) Unified fit<sup>29,30</sup> to the calculated Casassa form factor for linear  $R_{g,l} = 100$ .  $G = 1$ ,  $R_g = 71.1$ ,  $B_f = 1.54$ , and  $d_f = 2.12$ .

than 2 due to the constraint of the cyclic structure.  $d_f$  in Table 1 displays a value close to 2.12 for all of the samples. We expect  $d_f$  to also approach 2 for very high molecular weights.  $c$ , in Table 2, decreases with molecular weight toward a value of 1 expected for a linear chain. For all of the samples  $\phi_{Br}$  is close to the expected value of 0.5.  $\phi_M$  increases with increasing chain length as the chains become more convoluted with the relaxation of the cyclic constraint at high  $z$ .

Figure 3 compares values of the connectivity dimension,  $c$ ,  $d_{min}$ , and  $d_f$  from Table 2 with  $z$  from eq 13 using  $k = 1.89$  which is the best fit to eq 7. Equations 7 and 8 (using  $d_f = 2.12$ ) as well as a line of value 2.12 are also plotted. At about  $z = 3.7$ ,  $c = d_f \approx 2.12$ , and  $d_{min} \approx 1$  indicating close to an extrapolated disk structure. At high  $z$ ,  $c$  asymptotically approaches 1 for a linear chain. The functionality of  $d_f$  is not predicted but values close to 2.12 are observed for low  $z$ . Figure 3 does not indicate cyclic collapse at high  $z$  because the data is well represented by eqs 7 and 8. For cyclic collapse we would expect a deviation from eqs 7 and 8 toward an increase in  $c$  and a decrease in  $d_{min}$  at high  $z$ .

### Casassa Equation

The Casassa form factor for cyclics is given by,<sup>20</sup>

$$P(q) = \frac{1}{t} \exp(-t^2) \int_0^t \exp(x^2) dx = \frac{1}{t} \text{Daw}(t) \quad (14)$$

where  $t = qR_{g,l}/2$ , and  $R_{g,l}$  is the radius of gyration for a linear chain of the same molar mass as the cyclic under Gaussian scaling conditions,  $d_f = 2$ .  $\text{Daw}(t)$  in eq 14 is the Dawson integral of  $t$  that extrapolates to a value of  $t$  at low- $qR_{g,l}$ . Equation 14 is plotted in Figure 4. In some cases it has been reported that the Casassa equation does not accurately predict measured scattering data from cyclics, especially for higher molecular weight cyclics.<sup>12,13</sup> As an alternative, some authors<sup>12,13</sup> have even used the Debye function<sup>28</sup> for linear polymer chains to attempt to fit cyclic SANS data with equally poor results. The unsatisfactory fits obtained using the Casassa equation, according to the authors of these reports, is possibly related to contamination with linear chains. The scaling model indicates that a more fundamental problem exists with the Casassa equation as outlined below.

Calculations based on the Casassa function are shown in Figure 4a for a series of cyclics of variable linear chain  $R_{g,l}$ 's that are listed in the legend. The intermediate- $q$  (approximately  $4 < qR_{g,l} < 14$ ) power-law slope of all of these calculations is identical. The curves superimpose on the  $R_{g,l} = 100$  curve if the  $q$  vector is multiplied by  $R_{g,l}/100$ . Such scaling does not affect the topology of the structures so that  $c$ ,  $d_{min}$ , and  $d_f$  are identical

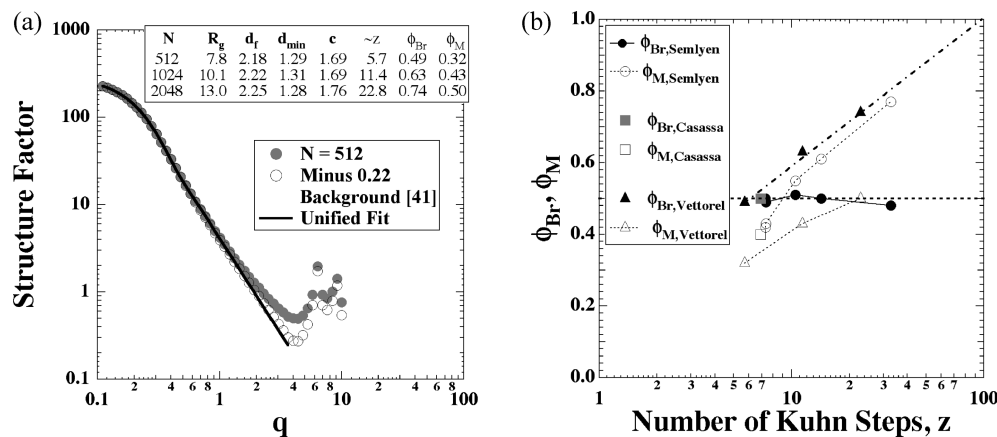


**Figure 5.** (a) Unified fit to structure factor calculated by Vettorel, Grosberg and Kremer. Structure factor is for a cyclic of 512 units. Inset shows fit and calculated results for three molecular weights shown in ref 15. Data is digitized from the inset to Figure 9 in Vettorel et al.<sup>15</sup> (b)  $\phi_{Br}$  and  $\phi_M$  for the experimental data of Semlyen's group,<sup>12-14</sup> the Casassa eq 14 and the simulations of Vettorel, Grosberg, and Kremer<sup>15</sup> versus the log of  $z$ .

for all of the scattering curves calculated by eq 14. The  $R_{g,l} = 100$  curve is fit in Figure 4b resulting in  $d_f \approx 2.12$ ,  $d_{min} \approx 1.36$ , and  $c \approx 1.56$ . These values vary somewhat with the fitting range in  $q$ . If the Casassa value for  $c$  is used in eq 7 a value for  $z$  of 6.9 is obtained as shown by the dashed vertical line in Figure 3. The high- $q$  behavior of the Casassa equation, Figure 4b at  $q \sim 0.4$ , displays a rapid decay that is not related to the structure of the cyclic. For this reason, the Casassa equation is valid only for a limited range of about  $q < 10/R_g$ , and can only strictly meet the conditions of a cyclic,  $p = z/2$ , for a fixed value of  $z \approx 6.9$  although the Casassa function displays close to the expected behavior for low molar mass cyclics.

### Calculated Cyclic Structure Factors

Vettorel, Grosberg and Kremer have simulated low molecular weight, unconcatenated cyclic melts using a lattice based Monte Carlo model<sup>15</sup>. The results show good convergence for different initial configurations indicating that the approach is ergodic. For simulations of cyclics with more than about 1000 units the scaling of coil size with number of units,  $N$ , seems to follow 3d behavior,  $R^3 \sim N$ , indicating coil collapse at high  $N$  due to conformational restrictions associated with topology as discussed above.<sup>7,8,15-18</sup> Vettorel<sup>15</sup> has provided structure factors calculated from the equilibrated coil structures at three different chain lengths, 512, 1024, and 2048 units.

Figure 5a shows the digitized structure factor for a 512 unit cyclic from ref 15. The structure factor displays features relating to the lattice at high- $q$  that interfere with the scaling regime. This can be approximately removed through the subtraction of a flat background of 0.22.<sup>41</sup> The Unified fit well represents the corrected structure factor and results in the radius of gyration and dimensions listed in the inset to Figure 5a. Similar fits (using 0.22 as a substructural background) result in the values for  $N = 1024$  and 2048 that are also listed in the inset to Figure 5a.

Since the number of units in a Kuhn length of the simulated structure is not known,  $z$  for these simulated cyclics can not be directly obtained. However, the calculated  $c$  and  $d_{min}$  values for 512 units roughly agree with the expected values at  $z \sim 5.7$  in Figure 3, indicating about 90 units per Kuhn length. This would appear to represent a rather rigid backbone for these simulated cyclics. The mass-fractal dimension in FIGS. 3 and 5a differ making this comparison somewhat inaccurate.

The values in the inset table of Figure 5a support coil collapse at high  $N$ . An uncollapsed cyclic will follow eq 7, so it is expected that  $c$  will decrease with  $N$ . Similarly,  $d_{min}$  should increase for higher  $N$  following eq 8. This behavior is roughly seen in comparing  $N = 512$  and 1024. However, at the highest  $N$  the

behavior is reversed. An increase in  $c$  with  $N$  for a cyclic can only be achieved by chemical reaction that leads to enhanced connectivity such as branching; or by coil collapse such as occurs in biomolecular folding.<sup>24</sup> Therefore, the proposition of Vettorel et al. that the simulated cyclics may collapse to a globular structure at high  $N$ <sup>15-18</sup> is supported by the scaling model analysis of the published structure factors.

Figure 5b plots  $\phi_{Br}$  and  $\phi_M$  for the experimental data of Semlyen's group,<sup>12-14</sup> the Casassa function and the simulated cyclics of Vettorel.<sup>15</sup> As mentioned above,  $\phi_{Br}$  displays a constant value of about 0.5 for the experimental data of Semlyen and for the Casassa equation consistent with uncollapsed cyclics. For Semlyen's experiments  $\phi_M$  increases with  $Z$  indicating that the cyclics display a more convoluted structure at higher molecular weights. The Casassa value for  $\phi_M$  agrees with the dependence seen for the Semlyen results. For Vettorel et al.'s simulations the cyclics display a consistent  $\phi_{Br}$  and  $\phi_M$  for the 512 point but diverge with less tortuosity for higher  $Z$  consistent with a partially folded or collapsed structure.<sup>24</sup> For folded structures there exist short circuits through the collapsed points that lead to a more direct average minimum path through the structure and a lower  $\phi_M$ .  $\phi_{Br}$  deviates significantly from 0.5 for the higher  $N$  simulations indicating enhanced connectivity in the higher molecular weight simulations.  $\phi_{Br}$  seems to follow close to a linear dependence in  $\log(z)$  allowing for a rough extrapolation to  $\phi_{Br} = 1$  for a collapsed (or folded) structure.<sup>24</sup> This crude extrapolation predicts a collapsed structure at roughly  $z = 97$  or  $N = 8700$  units for the simulated cyclics. It is unclear if this extrapolation is valid with only three data points over a rather narrow range of  $z$ .

### Conclusion

A new scaling model for cyclic polymers was presented and applied to literature SANS data. The new analysis can characterize fundamental structural and thermodynamic features associated with cyclic macromolecules. It was demonstrated that uncollapsed cyclic structures, regardless of their size and molar mass, can be characterized by  $\phi_{Br} = 0.5$  as predicted by the model. This approach results not only in an effective description of cyclic structures in general, but also pinpoints problems with traditional approaches in the literature, viz. the Casassa form factor. The scaling model was also applied to simulation results showing coil collapse at high molecular weight. It was shown that the approach could be used to discern early stages of cyclic collapse due to topological constraints. Coil collapse was not seen in the experimental data. It is hoped that this approach could be used to further our understanding of a variety of structures encountered in biological as well as in synthetic cyclic molecules.

**Acknowledgment.** This work was supported by the NSF (CTS-0626063) and by a grant from Equistar Corporation. The application of scaling models to cyclics was suggested to the authors in discussions with S. J. Clarson and he is acknowledged and thanked for raising our interest in this area. Discussions with S. K. Sukumaran of Yamagata University, Yonezawa, Japan, were important to this manuscript.

## References and Notes

- (1) Hoefler, J. P.; Meyer, T. E.; Yun, Y.; Jameson, J. L.; Habener, J. *Science* **1988**, *242*, 1430–1433.
- (2) Takasawa, S.; Nata, K.; Yonekura, H.; Okamoto, H. *Science* **1993**, *259*, 370–373.
- (3) Atwood, J. L.; Holman, K. T.; Steed, J. W. *Chem. Commun.* **1996**, *12*, 1401–1407.
- (4) Dietz, M. L.; Dzielawa, J. A. *Chem. Commun.* **2001**, *20*, 2124–2125.
- (5) Deutman, A. B. C.; Monnereau, C.; Elemans, J. A. A. W.; Ercolani, G.; Nolte, R. J. M.; Rowan, A. E. *Science* **2008**, *322*, 1668–1671.
- (6) deGennes, P. G. *Scaling concepts in polymer physics*; Cornell Univ. Press: New York, 1979.
- (7) Cates, M. E.; Deutsch, J. M. *J. Phys. (Paris)* **1986**, *47*, 2121–2128.
- (8) Obukhov, S. P.; Rubinstein, M.; Duke, T. *Phys. Rev. Lett.* **1994**, *73*, 1263–1266.
- (9) McLeish, T. *Science* **2002**, *297*, 2005–2006.
- (10) Kapnistos, M.; Lang, M.; Vlassopoulos, D.; Pyckhout-Hintzen, W.; Richter, D.; Cho, D.; Chang, T.; Rubinstein, M. *Nat. Mater.* **2008**, *7*, 997–1002.
- (11) Nam, S.; Leisen, J.; Breedveld, V.; Beckham, H. W. *Macromolecules* **2009**, *42*, 3121–3128.
- (12) Arrighi, V.; Gagliardi, S.; Dagger, A. C.; Semlyen, J. A.; Higgins, J. S.; Shenton, M. J. *Macromolecules* **2004**, *37*, 8057–8065.
- (13) Gagliardi, S.; Arrighi, V.; Ferguson, R.; Dagger, A. C.; Semlyen, J. A.; Higgins, J. S. *J. Chem. Phys.* **2005**, *122*, 064904.
- (14) Gagliardi, S.; Arrighi, V.; Dagger, A.; Semlyen, A. J. *Appl. Phys. A: Mater. Sci. Process.* **2002**, *74* (Suppl.), S469–S471.
- (15) Vettorel, T.; Grosberg, A. Y.; Kremer, K. *Phys. Biol.* **2009**, *6*, 025013.
- (16) Mueller, M.; Wittmer, J. P.; Cates, M. E. *PRE* **2000**, *61*, 4078–4089.
- (17) Mueller, M.; Wittmer, J. P.; Cates, M. E. *PRE* **1996**, *53*, 5063–5074.
- (18) Hur, K.; Winkler, R. G.; Yoon, D. Y. *Macromolecules* **2006**, *39*, 3975–3977.
- (19) Bielawski, C. W.; Benitez, D.; Grubbs, R. H. *Science* **2002**, *297*, 2041–2044.
- (20) Casassa, E. *J. Polym. Sci. Part A* **1965**, *3*, 605–614.
- (21) Beaucage, G. *Phys. Rev. E* **2004**, *70*, 031401.
- (22) Kulkarni, A. S.; Beaucage, G. *Macromol. Rapid Commun.* **2007**, *28*, 1312–1316.
- (23) Kulkarni, A. S.; Beaucage, G. *J. Polym. Sci., Part B: Polym. Phys.* **2006**, *44*, 1395–1405.
- (24) Beaucage, G. *Biophys. J.* **2008**, *95*, 503–509.
- (25) Ramachandran, R.; Beaucage, G.; Kulkarni, A. S.; McFaddin, D.; Merrick-Mack, J.; Galiatsatos, V. *Macromolecules* **2008**, *41*, 9802–9806.
- (26) Ramachandran, R.; Beaucage, G.; Kulkarni, A. S.; McFaddin, D.; Merrick-Mack, J.; Galiatsatos, V. *Macromolecules* **2009**, *42*, 4746–4750.
- (27) Edwards, C. J. C.; Richards, R. W.; Stepto, R. F. T.; Dodgson, K.; Higgins, J. S.; Semlyen, J. A. *Polymer* **1984**, *25*, 365–368.
- (28) Higgins, J. S.; Benoit, H. C. *Polymers and Neutron Scattering*; Oxford Science Publications: New York, 1994.
- (29) Beaucage, G. *J. Appl. Crystallogr.* **1995**, *28*, 717–728.
- (30) Beaucage, G. *J. Appl. Crystallogr.* **1996**, *29*, 134–146.
- (31) Beaucage, G.; Kammler, H. K.; Mueller, R.; Strobel, R.; Agashe, N.; Pratsinis, S. E.; Narayanan, T. *Nat. Mater.* **2004**, *3*, 370–374.
- (32) The appropriateness of the athermal simplification can be assessed by considering the change in  $I(0)$  due to excluding the interaction parameter for linear 15 kg/mol PDMS in a H/D mixture of 50% volume fraction which is about 4.5% from the values given by Beaucage et al.<sup>33</sup> This effect diminishes with increase in scattering vector and with reduction in the molecular weight. The absolute intensity measurement is generally good to about 10%. For the samples listed in Tables 1 and 2, the impact of the athermal assumption is not particularly significant. The interaction parameter should be considered for higher molecular weight blends, for example for 75 kg/mol blends  $I(0)$  changes by 33%.<sup>33</sup> In order to include the interaction parameter the Unified function could be included as the structure factor in the RPA equation for example.
- (33) Beaucage, G.; Sukumaran, S.; Clarson, S. J.; Kent, M. S.; Schaefer, D. W. *Macromolecules* **1996**, *29*, 8349–8356.
- (34) A single  $R_g$  value has been reported in Table 1 from the fits and because the model assumes that the H and D components have the same radius of gyration. However, some of the H/D mixtures in Table 1 are asymmetric. The model can be extended to account for polydispersity through the use of an additional parameter as proposed by Sorensen and Wang,  $C_p$ ,<sup>35</sup>  $C_p$  for Gaussian chains is equivalent to the ratio of  $M_z/M_w$  as described by Ramachandran et al.<sup>25</sup> The molecular weights for PDMS 3 in Table 1 are particularly asymmetric. For this blend we can calculate  $M_z/M_w$ , considering monodisperse components, as 1.03 (while  $M_w/M_n = 1.17$ ). This “worst case” value will shift  $d_{min}$  from 1.51 to 1.47, and  $z$  from 10.5 to 9.9 while  $c$  is unchanged, and  $\phi_B$  changes from 0.51 to 0.50. Hence, the scaling model is fairly insensitive to polydispersity in the range of molecular weights studied here.
- (35) Sorensen, C. M.; Wang, G. M. *PRE* **1999**, *60*, 7143–7148.
- (36) Flory, P. J. *Statistical Mechanics of Chain Molecules*; Interscience: New York, 1969; p 174.
- (37) Lapp, A.; Picot, C.; Benoit, H. *Macromolecules* **1985**, *18*, 2437.
- (38) Schultz, G. V.; Haug, A. Z. *Phys. Chem. (Frankfurt)* **1962**, *34*, 328.
- (39) Lapp, A.; Strazielle, C. *Makromol. Chem., Rapid Commun.* **1985**, *6*, 591.
- (40) Rai, D. K.; Ramachandran, R.; Beaucage, G. *Macromol. Rapid Commun.* **2009**, submitted for publication.
- (41) Scattering from the lattice structure will lead to a finite  $I(0)$  value just as light scattering from nanoscale molecules leads to a finite  $I(0)$  at  $qR_g \ll 1$ . In light scattering this constant intensity is used to calculate the weight average molecular weight from a static light scattering measurement. The  $I(0)$  associated with lattice scattering in Figure 5a leads to an excess intensity of about 0.22 that should be subtracted to obtain a reasonable power-law regime for the coil scattering. Here, 0.22 was determined by inspection of the corrected scattering curve compared to the expected power-law dependence of arbitrary slope  $-d_f$  in Figure 5a. This inherent “background” is also important in experimental determination of the structure factor at high- $q$  and can be experimentally quantified through high- $q$  measurements in the diffraction regime.